Chemical Engineering Journal 151 (2009) 286–294

Contents lists available at ScienceDirect

Chemical Engineering Journal

journal homepage: www.elsevier.com/locate/cej

Incorporation of Eulerian–Eulerian CFD framework in mathematical modeling of chemical absorption of acid gases into methyl diethanol amine on sieve trays

M. Baniadam, J. Fathikalajahi*, M.R. Rahimpour

Chemical and Petroleum Engineering Department, Shiraz University, Namazi, Shiraz 7134 851154, Iran

ARTICLE INFO

Article history:
Received 2 October 2007
Received in revised form 15 June 2008
Accepted 3 March 2009

Keywords:
Gas absorption
Computational fluid dynamics
Gas sweetening

ABSTRACT

A two-dimensional mathematical model for removal of acid gases (H_2S and CO_2) by methyl diethanol amine in a commercial sieve tray column has been developed. The velocity profile in the liquid both in radial and axial directions of each plate has been calculated by Eulerian–Eulerian computational fluid dynamics framework. In order to establish the temperature and concentration profiles in radial and axial directions of plates, mass and energy balance equations have been developed and solved numerically. A non-equilibrium rate based method combined with the two-film theory has been considered to obtain concentration profile. In this model most of the important parameters in the gas absorption process have been included, therefore one can expect that the model will be able to predict the performance of the columns at wide ranges of operating conditions. The results obtained by the model using operational data of a commercial plant indicate that there exists appreciable distribution of velocity, concentration and temperature in radial and axial directions. More interesting finding is that the extent of these distributions decline from bottom to top of the column as is expected. In fact, good agreement was noticed when the results of model were compared with operating conditions of an industrial column.

1. Introduction

Natural gas is considered sour if it contains H_2S and CO_2. Before the gas can be used, these acid gases should be removed by sweetening process. In this processes usually N.G. is sweetened by separation of H_2S and CO_2 in a sieve plate or packed type columns. In these columns, usually the gas and amine get in contact by a counter-current flow pattern in order to transfer these gases into the amine.

The gas absorption is a well-known technique and it is one of the most common method for separation of acid gases in gas refineries. Although this method is energy intensive, nevertheless it is the first choice among different separation techniques. Alkanolamines are widely used for purposes of separation of acid gases from natural gas. These amines have high ability to absorb the acid gases because the chemical reactions between the alkanolamines and these gases create a good driving force, which is necessary for absorption process. Since these chemical reactions are reversible, therefore, the alkanolamines can be recovered easily.

The occurrence of ionic reactions in one hand and lack of information about the tray hydraulics in the other hand raise a challenging design task. There are enough evidence that in the commercial size trays there exist velocity, concentration and temperature gradients in the radial direction. These non-uniform distributions not only reduce efficiency but also inaccurate prediction of column performance will be obtained once they are ignored. In order to account for these mal-distributions in the model one should incorporate the fundamental concepts of fluid mechanics. In fact, in the most of previous studies the fluid mechanics have been ignored altogether [1–3]. One reason for the reluctance to approach the modeling in a more fundamental way is the difficulty of solving the large and complex equations of two- or three-dimensional multi-phase systems.

For a given set of operating conditions (gas and liquid flows), tray geometry (column diameter, weir height, weir length, diameter of holes, fractional hole area, active bubbling area, downcomer area) and system properties, it is required to predict the fluid flow on the tray, residence time distributions and the mass transfer rates in each fluid phase.

One of the major assumptions made in modeling of distillation and gas absorption processes is considering each tray as an equilibrium stage (liquid and vapor streams leaving the tray are at equilibrium) and usually hydrodynamics of the tray is neglected. Neglecting this phenomenon shadows the predicted parameters in the large scale tray based on efficiency of a small scale tray. The inadequacy in the models to some extent was corrected by using the concept of (a) tray Murphree efficiency or (b) by non-equilibrium concepts [4]. Currently the most common assumption in distillation and absorption models is the concept of the fully mixed

* Corresponding author. Tel.: +98 711 2303071; fax: +98 711 6287294.
E-mail address: fathi@squ.edu.om (J. Fathikalajahi).

1385-8947/$ – see front matter © 2009 Elsevier B.V. All rights reserved.
doi:10.1016/j.cej.2009.03.004

Nomenclature

a	interfacial area (m^{-1})
A	tray area (m^2)
A_1	dimensionless concentration of CO_2 in the liquid film
A_2	dimensionless concentration of H_2S in the liquid film
B_2	dimensionless concentration of MDEA in the liquid film
A_h	hole area (m^2)
C	concentration (kg/m^3), (mol/m^3)
C_D	drag coefficient
C_p	specific heat (J/mol K)
d_G	diameter of bubble (m)
D	diffusivity (m^2/s)
De	Eddy diffusivity (m^2/s)
E	enhancement factor
E_2	dimensionless concentration of HCO_3^- in the liquid film
E_3	dimensionless concentration of HS^- in the liquid film
F_2	dimensionless concentration of $MDEAH^+$ in the liquid film
G	dimensionless group defined in Table 2
$\mathbf{g}$	vector of gravity acceleration (m/s^2)
H	specific enthalpy (J/mol)
h	molar enthalpy (J/mol)
h_{cl}	clear liquid height (m)
h_f	froth height (m)
h_w	weir height (m)
k_l°	mass transfer coefficient (m/s)
L	molar flow rate of liquid phase (mol/s)
l_{mix}	Prandtl mixing length (m)
L_w	weir length (m)
$\mathbf{M}_{L.G}$	interphase momentum transfer ($kg/m^2\ s^2$)
P	pressure (Pa)
p_i	dimensionless concentration of species defined in Table 2
Q	volumetric flow rate (m^3/s)
R_{MDEA}	dimensionless reaction rate of CO_2 and MDEA defined in Table 2
$r_{p,k}$	interface momentum transfer caused by mass transfer ($kg/m^2\ s^2$)
Sc	Schmidt number
pi	dimensionless diffusivity of species defined in Table 2
T	temperature (K)
u	x-component of velocity (m/s)
U	superficial velocity (m/s)
v	velocity vector (m/s)
v_{slip}	sleep velocity (m/s)
v	y-component of velocity (m/s)
V	molar flow rate of gas phase (mol/s)
w	z-component of velocity (m/s)
x	Cartesian coordinate, mole fraction of liquid phase
y	Cartesian coordinate, mole fraction of gas phase
z	Cartesian coordinate, only is defined for liquid film geometry (m)

Greek symbols

α	molecular temperature conductivity (m^2/s)
δ	film thickness (m)
φ	volume fraction of each phase
Γ	interphase mass transfer ($kg/m^2\ s$)
μ	dynamic viscosity (kg/m s)
ν	kinematic viscosity (m^2/s)
ρ	density (kg/m^3)
τ	shear stress (Pa)
τ'	Reynolds stress (Pa)
ξ	dimensionless distance from liquid interface

Superscripts

abs	absorption
liq	referring to liquid phase
vap	referring to gas phase
tr	transpose

Subscripts

avg	average
blk	bulk
G	referring to gas phase
k	phase number
L	referring to gas phase
ref	reference
t	turbulence
wall	tray wall

ideal tray—i.e. spatial variations in concentration, temperature and velocity are ignored.

In recent years, advancements have been made by applying CFD for simulating the liquid flow on a tray by means of various theoretical models, such as the stream function model [5], the k–ε turbulence model [6] and the two-fluid turbulence model [7].

Several investigators have attempted to include the hydrodynamics of plate in the model by using CFD [8–12]. Although the previous models are able to give satisfactory results for the velocity profile at different liquid rates, but they have overlooked effect of chemical reactions in the liquid. The vapor–liquid flow on a tray is also characterized by cross flow of the two phases. In this theory, the liquid phase is usually considered as continuous phase and the upward vapor flow is supposed to be dispersed phase [9].

Mehta et al. [8] have analyzed the liquid phase flow patterns on a sieve tray by solving the time-averaged equations of transport only for the liquid. Interactions with the vapor phase are taken into account using of interphase momentum transfer coefficients determined from empirical correlations. Yu et al. [12] attempted to model the two-phase flow behavior using a two-dimensional model, focusing on the description of the hydrodynamics along the liquid flow path, ignoring the velocity profile of gas along the height of the plate. Fischer and Quarini [10] have attempted to describe the three-dimensional transient gas–liquid hydrodynamics. An important key assumption made in the simulations of Fischer and Quarini concerns the interphase momentum exchange (drag) coefficient; these authors assumed a constant drag coefficient of 0.44, which is appropriate for uniform bubbly flow. This drag coefficient is not appropriate for description of the hydrodynamics of trays operating in either the froth or spray regimes.

van Baten and Krishna [11] developed a three-dimensional transient CFD model, within the two-phase Eulerian framework, to describe the hydrodynamics of a sieve tray. The required exchange coefficient of interphase momentum transfer is estimated based on the correlation of Bennett et al. [13] for the liquid hold-up. Krishna has carried out his simulations with varying superficial gas velocity, liquid weir loads, and weir heights.

There are yet other excellent surveys of the literature in this area [14]. Literature contains correlations for tray hydrodynamics which

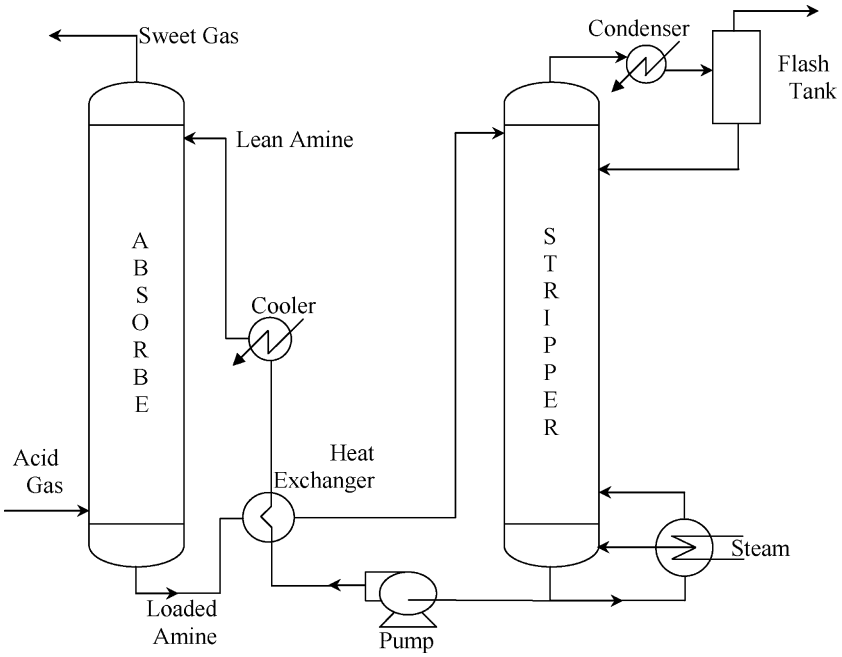

Fig. 1. Simplified flow diagram of an acid gas-alkanolamine unit.

are largely empirical in nature. In a recent policy document on separations gathered by a group of industry and university experts, a lack of in-depth understanding of the processes occurring within a distillation column was believed to be a significant barrier to the further improvement of equipment performance. The experts cited transport phenomena such as fluid flow, heat and mass transfer, and multi-phase flow as subjects that are insufficiently understood [15].

Material and energy balance equations are common to all methods. There are equilibrium and non-equilibrium models of separation process in the column. Drawback of non-equilibrium models [16,17] are complication of calculating driving forces for mass and energy balance where flow structures is considered. Higler et al. have developed a non-equilibrium model for reactive distillation by using a cell approach [18–22].

In this study a new two-dimensional mathematical model for absorption of CO_2 and H_2S from natural gas using solutions of alkanolamines has been developed. In this model tray space is discretized as a set of cells in axial and radial directions and velocity profile of liquid is calculated at each point of the tray. In each cell energy equation and mass transfer equations including reactions are written according to the two-film theory across the liquid film. In comparison with Higler's cell model for reactive distillation in which equal flow rates were assumed to all cells of the tray, in this model we have used his idea and divided the plate space to many cubic cells with different flow rates.

2. Gas sweetening plant

A typical gas sweetening unit is shown in Fig. 1. The unit consists of two tray or packed towers namely, the absorber and the stripper. The acid gas is introduced at the bottom of the absorber generally at pressure ranges of 10–70 bar, and contacts counter-currently the lean amine solutions, which enters at the top of absorber at temperatures varying between 30 and 50 °C. The amine solution, which leaves the bottom of the absorber loaded with the acid gas, is heated by the lean amine solution leaving the bottom of the stripper. The loaded or rich solution is then introduced at the top of the stripper. Steam is introduced at the bottom of the stripper to decrease the partial pressure of the acid gas and supply the heat necessary to enhance the reverse reactions.

The concentrated acid gas stream leaving the top of the stripper is cooled and flashed to recover the steam and the vaporized amine. The condensate is refluxed to the top of the stripper. The stripper usually operates at low pressure (below 1 bar) and high temperature (100–120 °C).

3. Mathematical modeling

Modeling two-phase flow requires the use of appropriate conservation equations that can account for the behavior of each phase and the interactions between them. In this work, the two-fluid model of Ishii [23] is used.

The foundation for the two-fluid model is the local instantaneous formulation of the momentum and continuity equations on a continuum scale. Two-phase flow is visualized as a "number of single-phase regions bounded by moving interfaces" Ishii [23]. In the local instantaneous formulation, single-phase conservation equations are implemented in the continuous regions and jump conditions are used to match the phase interfaces. Each of the single-phase region obeys the general single-phase balance equations of mass, momentum, and energy. The two-fluid model is developed by taking an Eulerian time and volume average of the instantaneous formulation. High frequency fluctuations in flow are filtered out, leaving only the low frequency effects that are of interest [24].

In steady state conditions, each phase is also constrained by the volume-averaged continuity equation:

$$\nabla \cdot (\varphi_k \rho_k v_k) = \Gamma_k \quad k = 1, 2 \tag{1}$$

The interfacial mass transfer, Γ_k, is constrained by the overall conservation of mass law. The volume-averaged momentum balance equation can be expressed as follows:

$$\nabla \cdot (\varphi_k \rho_k v_k v_k) = -\nabla(\varphi_k P_k) + \nabla \cdot (\varphi_k(\boldsymbol{\tau}_k + \boldsymbol{\tau}_k^t)) + \varphi_k \rho_k \boldsymbol{g} + \boldsymbol{M}_{LG} \tag{2}$$

The terms on the left hand side of Eq. (2) account for the convective acceleration. The terms on the right hand side account for the

pressure (P_k), the viscous stress ($\boldsymbol{\tau}_k$), Reynolds stresses ($\boldsymbol{\tau}_k^t$), body forces ($\rho_k \mathbf{g}$), and interfacial momentum transfer ($\mathbf{M}_{LG}$), respectively.

On industrial size sieve trays, the froth height is typically an order of magnitude smaller than the tray diameter (a typical froth height is in the order of 0.2 m; a typical industrial column diameter is in the order of 2.0–5.0 m). In addition, the velocity of gas rising in the vertical direction is much greater than the velocity of the liquid flowing across the tray deck. Because of these two reasons, the gas residence time in the froth zone is much shorter than the liquid residence time. Due to the short residence times, it can be assumed that the gas moves through the froth in a plug flow pattern [24].

The viscous stress term $\boldsymbol{\tau}_k$, is most commonly modeled using the assumption that each phase is a Newtonian fluid:

$$\boldsymbol{\tau}_k = \mu_k(\nabla.v_k + (\nabla.v_k)^{tr}) \tag{3}$$

The turbulent stress is evaluated using an equation with the same form as the viscous stress calculation, Eq. (3):

$$\boldsymbol{\tau}'_k = \mu_{k,t}(\nabla.v_k + (\nabla.v_k)^{tr}) \tag{4}$$

The equations used for the single-phase formulation are derived from Ishii's two-fluid formulation that is described previously. The phase momentum balance equation, Eq. (2) is combined with Eqs. (3) and (4) to give the following equation:

$$\nabla.(\varphi_k\rho_k v_k v_k) = -\nabla(\varphi_k P_k) + \nabla.(\varphi_k \mu_{effective,L}(\nabla.v_{\mathbf{L}} + (\nabla.v_{\mathbf{L}})^{tr})) + \varphi_k\rho_k \boldsymbol{g} + \boldsymbol{M}_{L.G} \tag{5}$$

where

$$\mu_{effective,L} = \mu_L + \mu_{L,t} \tag{6}$$

Term $\mathbf{M}_{L.G}$ includes two effects. The first is momentum mass transfer due to interfacial mass transfer and the second is momentum transfer based on drag between the two phases. This can be shown by the following equation:

$$\boldsymbol{M}_{L.G} = v_{k,s}\Gamma_k + r_{p,k} \tag{7}$$

The gas and liquid phases share the same pressure field, $P_G = P_L$. The effect of interphase mass transfer on momentum transfer between phases has been ignored in the present analysis. The interphase momentum exchange (drag) coefficient is estimated using the Bennett et al. [13] correlation as basis. For gas–liquid bubbly flows the interphase momentum exchange term is

$$\boldsymbol{M}_{L.G} = \frac{3}{4}\rho_L \frac{\varphi_{G,avg}}{d_G} C_D(u_G - u_L)|u_G - u_L| \tag{8}$$

For the churn-turbulent regime of bubble column operation, Krishna et al. [25] estimated the drag coefficient for a swarm of large bubbles using

$$C_D = \frac{4}{3}\frac{\rho_L - \rho_G}{\rho_L} g d_G \frac{1}{v_{slip}^2} \tag{9}$$

where v_{slip} is the slip velocity of the bubble swarm with respect to the liquid

$$v_{slip} = |u_G - u_L| \tag{10}$$

Substituting Eqs. (9) and (10) into Eq. (8) results

$$\boldsymbol{M}_{L.G} = \varphi_{G,avg}(\rho_G - \rho_L)g \frac{1}{v_{slip}^2}(u_G - u_L)|u_G - u_L| \tag{11}$$

The slip between gas and liquid can be estimated from superficial gas velocity U_G and the gas hold-up $\varphi_{G,avg}$

$$v_{slip} = \frac{U_G}{\varphi_{G,avg}} \tag{12}$$

After some rearrangements van Baten and Krishna presented the interphase momentum exchange term in the following form [11]:

$$\mathbf{M}_{L.G} = \varphi_{G,avg}\varphi_{L,avg}(\rho_L - \rho_G)g \times \left[\frac{1}{(U_G/\varphi_{G,avg})^2 \varphi_{L,avg}}\right](u_G - u_L)|u_G - u_L| \tag{13}$$

All of the turbulence models developed for single and two-phase flow have one or more fitted parameters. These parameters are determined from experimental study. Even the simplest and most limited turbulence model, the Prandtl mixing length model, has a single fitted parameter, l_{mix}. For the distillation system, there is simply not enough data to correlate the required parameters.

A more limited model can be implemented in order to develop a predictive model for turbulent viscosity. In this model, a turbulent Schmidt number is defined:

$$Sc_t = \frac{\mu_{t,L}}{\rho_L De} \tag{14}$$

Zuiderweg proposed the following eddy diffusivity correlation for spray mixed froth regime flows [26]:

$$De = \frac{8.3\rho_G u_s^2 h_{cl}^2}{\rho_L(Q_L/L_w)} \tag{15}$$

where L_w is weir length. Zuiderweg also proposed a correlation for emulsion regime flows:

$$De = 3.0\, u_s h_{cl}\left(\frac{\rho_G}{\rho_L}\right)^{0.5} \tag{16}$$

If it is assumed that the flows are highly mixed, the turbulent Schmidt number can be assumed equal to one. Thus, the turbulent viscosity is equal to the product of density and eddy diffusivity [24]. The clear liquid height, h_{cl}, which is used in Eqs. (15) and (16) is calculated by the method proposed by Bennett et al. [13].

Here the simplifications that are introduced by V.A. Danilov are made in order to have equations that are more convenient for solution [17]. They accepted froth regime of tray to be characterized with well developed turbulence in liquid phase which gives full mixing along height ($\partial C_L/\partial z = 0$, $\partial u_L/\partial z = 0$, $\partial \Gamma_L/\partial z = 0$). Turbulence in the bulk of liquid phase is accepted isotropic ($\nu_L^T = const$) and thermal properties changing are insignificant.

The equations of momentum transfer for liquid phase are then written in two-dimensional form as

$$u_L\frac{\partial u_L}{\partial x} + v_L\frac{\partial u_L}{\partial y} = -\frac{1}{\rho_L}\frac{\partial P}{\partial x} + \nu_{t,L}\frac{\partial^2 u_L}{\partial x^2} + \nu_{t,L}\frac{\partial^2 u_L}{\partial y^2} + \frac{\boldsymbol{M}_{L.G,x}}{\rho_L} \tag{17}$$

$$u_L\frac{\partial v_L}{\partial x} + v_L\frac{\partial v_L}{\partial y} = -\frac{1}{\rho_L}\frac{\partial P}{\partial y} + \nu_{t,L}\frac{\partial^2 v_L}{\partial x^2} + \nu_{t,L}\frac{\partial^2 v_L}{\partial y^2} + \frac{\boldsymbol{M}_{L.G,y}}{\rho_L} \tag{18}$$

$$\frac{\partial u_L}{\partial x} + \frac{\partial v_L}{\partial x} = \frac{\Gamma_L}{\rho_L} \tag{19}$$

Boundary conditions for Eqs. (17)–(19) are set as follows:

$$x = 0, \qquad u_L = u_{L,0}, \qquad v_L = 0 \tag{20}$$

$$x = l, \qquad \frac{\partial u_L}{\partial x} = 0 \qquad \frac{\partial v_L}{\partial x} = 0 \tag{21}$$

$$y = 0, \qquad \frac{\partial u_L}{\partial y} = 0, \qquad v_L = 0 \tag{22}$$

$$y = y_{wall}(x), \qquad u_L = 0, \qquad v_L = 0 \tag{23}$$

The mass transfer of a gas into a reactive liquid follows a sequence of three steps: dissolution, diffusion, and reaction. The process can be best described using the two-film theory, which was developed, by Lewis and Whitman (Fig. 2) [27].

According to this theory, there exist a thin surface, gas–liquid interface, that separates the gas bulk from the liquid bulk and there

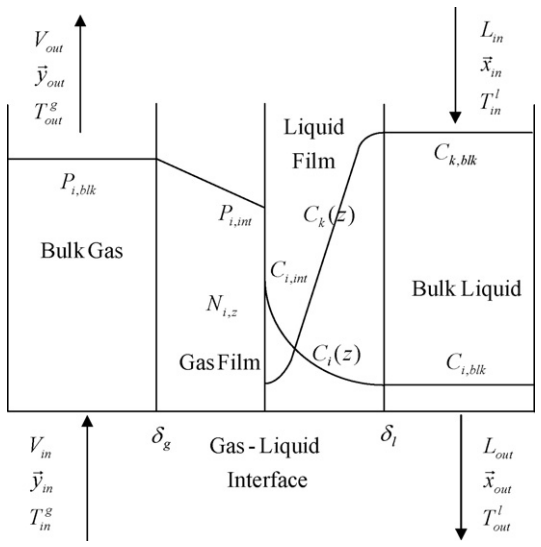

Fig. 2. Description of the two-film theory for reactive gas absorption process.

are two adjacent liquid and gas films. All the resistances to the mass and heat transfer process are assumed to occur in these films. Temperature of gas at the entrance is T^g_{in}, molar flow rate is V_{in}, and composition is $\vec{y}_{in}$. It contacts a liquid, with temperature of T^l_{in}, molar flow rate L_{in}, and composition $\vec{x}_{in}$. The diffusion process is one-dimensional and takes place perpendicular to interface; the gas–liquid interface is located at $z = 0$. Solute gas i crosses the interface into the liquid phase with a flux $N_{i,z}$. Due to the resistance in the gas phase, the concentration of the gas drops linearly from $P_{i,blk}$ in the gas bulk to $P_{i,int}$ at the gas liquid interface. The gas then dissolves in the liquid at the gas liquid interface where its concentration is given by $C_{i,int}$. It then diffuses and reacts with a liquid species k in the liquid film. As a result, the gas concentration drops to $C_{i,blk}$ at the edge of the liquid film. The concentration of the liquid species k also drops from $C_{k,blk}$ at the edge of the liquid film to $C_{k,int}$ at the gas liquid interface (Fig. 2).

The molar flux of the diffusing gas i must satisfy the following three relations:

$$N_{i,z} = \frac{V_{in}y_{i,in} - V_{out}y_{i,out}}{a} \tag{24}$$

$$N_{i,z} = k_{g,i}(P_{i,blk} - P_{i,\mathrm{int}}) \tag{25}$$

$$N_{i,z} = k^{\circ}_{l,i}E_i(C_{i,\mathrm{int}} - C_{i,blk}) \tag{26}$$

where a is the total area of the gas–liquid interface, are mass transfer coefficients of $k_{g,i}$ and $k^{\circ}_{l,i}$ species i in gas and liquid, respectively. E_i is the enhancement factor of mass transfer for species i. The latter corrects for the effect of chemical reactions on the gas absorption rate. Hence, it is defined as the ratio of gas flux calculated in the presence of chemical reaction to that which would happen in the absence of chemical reactions at the same driving force:

$$E_i = \frac{-D_i(dC_i/dz)|_{z=0} + r'_i\big|_{z=0}}{k^{\circ}_{l,i}(C_{i,\mathrm{int}} - C_{i,blk})} \tag{27}$$

where D_i is the diffusivity of the solute gas i in the solution and $r'_i\big|_{z=0}$ is the rate of surface reaction of gas i at the gas–liquid interface. This term is nonzero for only instantaneous reactions such as the reactions of the alkanolamine with H_2S.

Higler et al. [18–22] developed a non-equilibrium (NEQ) cell model to describe the operation of tray column. These assumptions are made in applying his model.

- Chemical reactions take place only in the liquid phase.
- Coupling between mass transfer and chemical reactions within the diffusion layer is accounted for.
- The use of multiple well-mixed cells in the liquid and vapor flow directions accounts for staging in either fluid phase.

In this study an improved form of Higler's cell model in steady state conditions has been applied to gas absorption process. In Higler's model the tray space is divided to several even cubes with the same gas and liquid entering flow rates. Since uniform distribution of flows into the cells is unlikely true because of velocity distribution across the plate, so in this work distribution of flow into the cells were considered based on actual velocities cells shown in Fig. 3. Mass balance for each species in this cell with different entering flow rates can be written in the following form:

$$N_{i,j} = V_{g,j,in}y_{i,j,in} - V_{g,j,out}y_{i,j,out}$$
$$= E_{i,j}aA'_jh_{cl}k_{l,i,j}(C_{i,j}|_{\mathrm{int}} - C_{i,j,blk}) + \sum_{k=1}^{4} D_i\frac{\partial C_{i,j,k}}{\partial z_k}A_{j,k} \tag{28}$$

where i stands for CO_2 and H_2S and j for each cubic cell. C is the concentration of each component in liquid, V_g is the volumetric flow rate of gas entering to cubic cell. Flow rate of gas is assumed to be distributed evenly. A'_j is the side area of each cubic cell and h_{cl} is the height of the cell. By k we mean each face of the cubic cell and $A_{j,k}$ is each face of cell.

These equations will be applied to all cubes that discrete the volume of tray in x and y directions. Liquid and gas enter to and exit from it in all four sides of cubes which are acting as a continuous stirred tank reactor (CSTR)

Governing equations in the liquid film can be resulted from combining the mass balance equation in the reacting film, charge balance in the liquid film and reaction equations between acid gases and MDEA. The final governing equations including five differential and one algebraic equation for the concentration of the six species CO_2 (A_1), H_2S (A_2), MDEA (B_2), HCO_3^- (E_2), HS^- (E_3), and $MDEAH^+$ (F_2) in the liquid film is written. The symbols in parenthesis are introduced to simplify the notations. The five differential equations and one algebraic equation obtained by material balance for

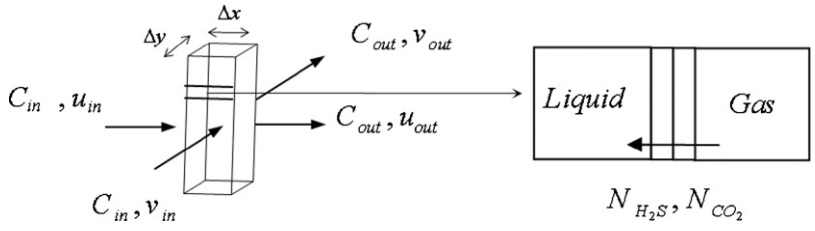

Fig. 3. Typical cell, for which conservation of mass and energy is written.

Table 1
Boundary conditions of governing equation on liquid film.

At $\xi = 0$ (gas–liquid interphase)

$$\frac{dA_1}{d\xi} + \beta_{A_1}\left(Y_{A_1,in} - \frac{y_{A_1,eq}A_1}{1-y_{w,eq}-y_{A_1,eq}A_1-y_{A_2,eq}A_2}\right) = 0$$

$$\frac{dA_2}{d\xi} - \left(\frac{s_{B_2}}{s_{A_2}p_{A_2}}\right)\frac{dB_2}{d\xi} + \beta_{A_2}\left(Y_{A_2,in} - \frac{y_{A_2,eq}A_2}{1-y_{w,eq}-y_{A_1,eq}A_1-y_{A_2,eq}A_2}\right) = 0$$

$$\frac{dE_2}{d\xi} = 0 \qquad \frac{dB_2}{d\xi} + \left(\frac{\bar{s}p_{E_3}}{s_{B_2}}\right)\frac{dE_3}{d\xi} = 0 \qquad A_2B_2 - E_3F_2 = 0$$

At $\xi = 1$ (edge of the liquid film)

$$A_1 = 1 \qquad A_2 = 1 \qquad B_2 = 1 \qquad E_2 = 1 \qquad E_3 = 1$$

Table 2
List of the dimensionless groups.

Dimensionless variables

$$A_1 = \frac{C_{A_1}}{C_{A_1,blk}} \qquad A_2 = \frac{C_{A_2}}{C_{A_2,blk}} \qquad B_2 = \frac{C_{B_2}}{C_{B_2,blk}}$$

$$E_2 = \frac{C_{E_2}}{C_{E_2,blk}} \qquad E_3 = \frac{C_{E_3}}{C_{E_3,blk}} \qquad F_2 = \frac{C_{F_2}}{C_{F_2,blk}}$$

$$\xi = \frac{z}{\delta_l} \qquad R_{MDEA} = \frac{\delta_l^2 r_{MDEA\text{-}CO_2}}{D_{A_1}C_{B_2,blk}}$$

$$G_1 = 0 \qquad G_2 = \frac{g_2}{C_{B_2,blk}} \qquad G_3 = \frac{g_3 D_{B_1}}{C_{B_1,blk}} \qquad G_4 = \frac{g_4 D_{B_2}}{C_{B_2,blk}} \qquad G_5 = \frac{g_5\delta_l^2}{C_{B_2,blk}^2}$$

Dimensionless parameters

$$q_i = \frac{C_{i,blk}}{C_{B_1,blk}} \qquad p_i = \frac{C_{i,blk}}{C_{B_2,blk}} \qquad s_i = \frac{D_i}{D_{A_1}} \qquad \bar{s} = \frac{\bar{D}}{D_{A_1}}$$

$$M_{MDEA} = \sqrt{k_l D_{A_1} C_{B_2,blk}/(k_{A_1}^{\circ})^2} \qquad \kappa_{MDEA} = \frac{k'_{R_1R_2R_3N}C_{B_2,blk}}{k'_{R_1R_2NH}C_{B_1,blk}}$$

$$\beta_{A_1} = \frac{V_l}{k_{A_1}^{\circ} a C_{A_1,blk}} \qquad \beta_{A_2} = \frac{V_l}{k_{A_2}^{\circ} a C_{A_2,blk}}$$

a system shown in Fig. 2 are [27]

$$\frac{d^2A_1}{d\xi^2} = -\frac{R_{MDEA}}{p_{A_1}} \tag{29}$$

$$\frac{d^2A_2}{d\xi^2} = \left(\frac{s_{B_2}}{s_{A_2}p_{A_2}}\right)\frac{d^2B_2}{d\xi^2} + \left(\frac{1}{s_{A_2}p_{A_2}}\right)R_{MDEA} \tag{30}$$

$$\frac{d^2B_2}{d\xi^2} = -\frac{G_4}{s_{B_2}G_2}R_{MDEA} - \frac{G_5}{G_2} \tag{31}$$

$$\frac{d^2E_2}{d\xi^2} = \frac{R_{MDEA}}{p_{E_2}\bar{s}} \tag{32}$$

$$\frac{d^2E_3}{d\xi^2} = -\left(\frac{s_{B_2}}{\bar{s}p_{E_3}}\right)\frac{d^2B_2}{d\xi^2} - \left(\frac{1}{\bar{s}p_{E_3}}\right)R_{MDEA} \tag{33}$$

$$F_2 = 1 + \frac{1}{p_{F_2}}[p_{E_2}(E_2-1) + p_{E_3}(E_3-1)] \tag{34}$$

Boundary conditions of governing equations in the liquid film and dimensionless groups are listed in Table 1 and Table 2 respectively.

4. Heat effects

The enthalpy of the gas, H^{vap}, and the liquid, H^{liq}, are given by [1]:

$$H^{vap} = V\sum_i y_i h_i^{vap} \tag{35}$$

$$H^{liq} = L\sum_i x_i h_i^{liq} \tag{36}$$

where h_i^{vap} and h_i^{liq} are the molar enthalpy of component i in the gas and liquid phase, respectively. These are given by

$$h_i^{vap} = h_{ref}(T_{ref}) + \bar{C}_{p,i}(T - T_{ref}) \tag{37}$$

For solvent H_2O, MEA, DEA and MDEA

$$h_i^{liq} = h_i^{vap} - (+\Delta h_i^{v}) \tag{38}$$

For dissolved CO_2 and H_2S

$$h_i^{liq} = h_i^{vap} - (-\Delta h_i^{abs}) \tag{39}$$

$$\sum_j \rho_l H_{l,j}\mathbf{V}_{l,j}.n_j + \rho_g(H_{g,in}V_{g,in} - H_{g,out}V_{g,out}) = 0 \tag{40}$$

where h_{ref} is the gas enthalpy at some reference temperature T_{ref}, and $\bar{C}_{p,i}$ the constant pressure ideal gas mean heat capacity and $+\Delta h_i^{v}$ and $-\Delta h_i^{abs}$ are the heats of vaporization and absorption of component i, respectively. The heat of absorption includes the effect of mixing and reaction. These equations assume ideality and are only applied to the molecular components. The effect of the ionic components on the liquid enthalpy is accounted for in the heat of absorption term.

5. Method of solution

After discretization a tray space as shown in Fig. 4, the following sequential steps were taken to solve Eqs. (17)–(40):

1. Eqs. (17)–(23) were solved on a tray in a two-dimensional space in order to calculate approximate velocity at each point. At this step zero was assigned for interphase mass transfer.
2. Having approximate velocities at surfaces of cubic cells from step 1, it was possible to write material and energy balance in each cell to establish Eqs. (28) and (40), respectively. Simultaneous solutions of these equations for all cells will give output streams from a tray provided that the enhancement factors are known. To find the enhancement factor for each cell the following two steps are necessary:
   (I) Enhancement factors for all cells in the first step was assumed to be one and the output streams from cells were calculated using Eqs. (24)–(26).
   (II) Having outputs from each cell, governing equations in the liquid film (29)–(34) were solved to obtain concentration profile in the liquid film. Once concentration profiles are in hand Eq. (27) will give new values for enhancement factors. These new values of enhancement factors are corrected in an iterative procedure from step I until convergence for enhancement factors are reached in each cell.
3. When enhancement factors are converged in all the cells, exact solution of Eqs. (17)–(23) would be possible in order to obtain the new velocity distribution in the liquid. The procedure was repeated from step 2 until difference in the velocities of two consecutive iterations was within a certain small range.

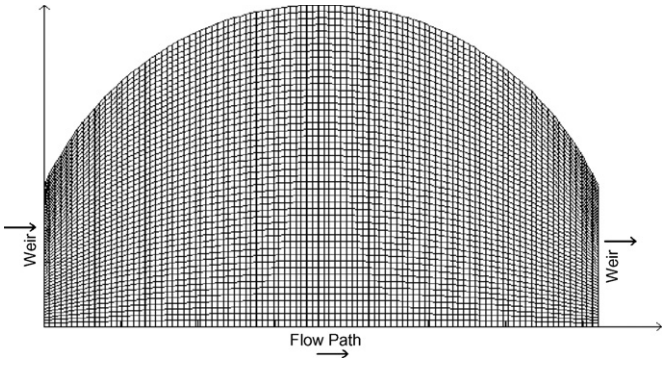

Fig. 4. Discretization of tray in x and y directions.

Table 3
Specifications of column and sieve trays.

Diameter	Height	No. of trays	Burble area	Active area	Diameter of holes	Weir height	Tray spacing
2.895 m	16.46 m	20	3393.5 cm^2	42411.96 cm^2	0.5556 cm	14.1 cm	80 cm

Table 4
Conditions of feed gas (sour) and lean amine streams.

	H_2S	CO_2	CH_4	H_2O	MDEA	Flowrate	Temperature (K)
Feed gas	4.00	6.54	89.43	0.03	–	7236.53 kmol h^{-1}	294.1
Lean amine	–	–	–	91.92	8.08	18453.49 kmol h^{-1}	327

Table 5
Comparison of model results and industrial data for sweet gas and rich amine.

	H_2S	CO_2	CH_4	H_2O	MDEA	F (kmol h^{-1})	T (K)
Sweet gas							
Model	3.8 ppm	2.47	97.24	0.29	–	6503.01	329.4
Industrial	4 ppm	2.55	97.16	0.29	–	6502.20	330
Rich amine							
Model	1.51	1.63	0.77	88.32	7.77	19187.02	350
Industrial	1.47	1.65	0.72	88.35	7.81	19188.11	350.5

6. Results and discussion

The model that explained in the previous sections, tested by operational data from an industrial plant. Design specifications of the absorber and representative input conditions of the sour gas and lean amine in the plant are summarized in Tables 3 and 4.

However the experimental data of inter-sections of this tower was not available and only end point results of operating tower can be compared with the results of presented mathematical model. This comparison is shown in Table 5.

Three representative trays, bottom tray (no. 1), middle tray (no. 10) and upper tray (no. 20), are considered to demonstrate velocity distribution. Temperature and concentration distribution are investigated in tray no. 1. Fig. 5 shows velocity distribution on mentioned trays. Trays are ordered from the bottom of the tower to the top in the direction of gas flow. Fig. 5 depicts appreciable variations of velocities of both direction and magnitude of velocity over the trays. The liquid velocity is higher in lower trays, because flow rate of liquid increase from top to bottom of the column. Lean amine absorbs acid gases during flowing from top to bottom and its flow rate increases. Higher velocity in the bottom trays increases the turbulency of liquid flow. In the upper trays we have two different regions for velocity distribution. Far from the tray wall, stream line of velocity is somewhat constant and they are nearly straight. According to the boundary conditions, both components of velocity (x component and y component) are zero on the contacting wall and this effect is preserved near the wall. As we move from the wall away to the center, shape of streamlines approaches to the straight lines. When we move toward the bottom of the absorption tower, the turbulence of liquid increases and it can be readily observed that in tray no. 1 velocity distribution is very complicated and vortexes are spread up to the middle of the tray.

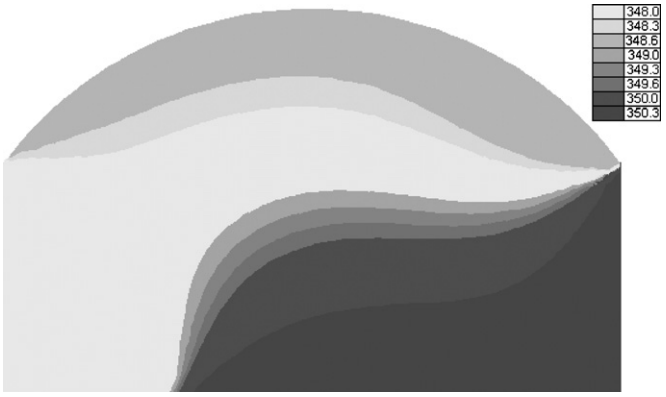

Fig. 6. Averaged temperature (K) distribution on tray no. 1.

The temperature distribution of tray is shown in Fig. 6. As one can see from this figure, temperature from entrance weir of tray to exit weir increases because of the chemical absorption of acid gases into MDEA and due to exothermic nature of reactions. However, according to Fig. 5, there are some areas near walls, where velocity is approximately zero. This phenomenon also is confirmed in Figs. 7 and 8. These areas have two distinct effect on concentration of H_2S and CO_2. Concentration of CO_2 increases near the wall while the concentration of H_2S decreases in that area. This difference in behavior of concentrations of H_2S and CO_2 near the walls can be due to the fact that the reaction between H_2S and MDEA is

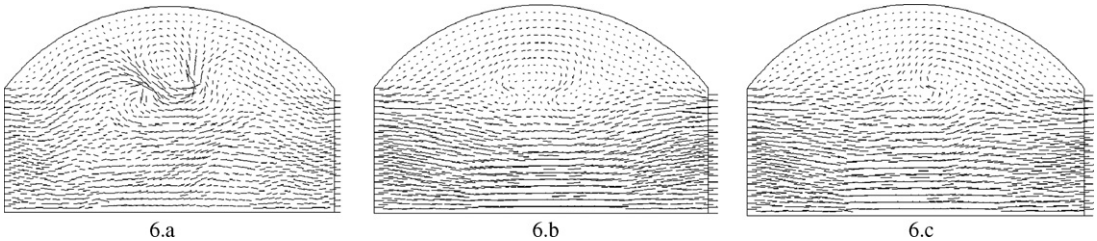

Fig. 5. Flow streams on tray no. 1: u_{L0} = 0.0845 m/s; tray no. 10: u_{L0} = 0.0785 m/s; tray 20: u_{L0} = 0.0778 m/s.

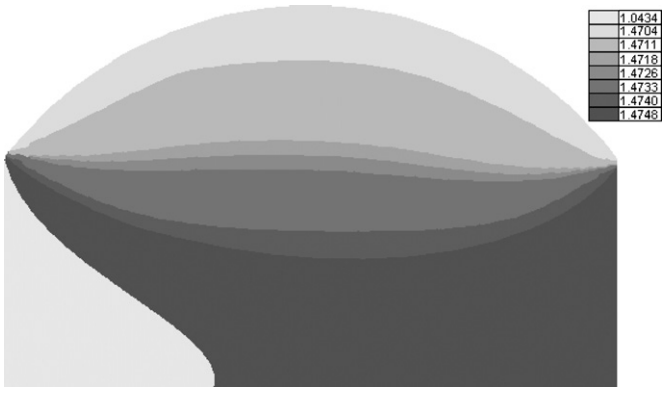

Fig. 7. Averaged distribution of mole percent of H_2S on tray no. 1.

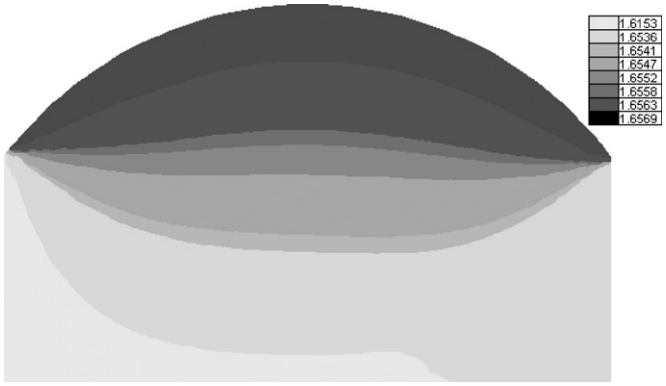

Fig. 8. Averaged distribution of mole percent of CO_2 on tray no. 1.

fast while the reaction between CO_2 and MDEA is not only slow but also it is a more stable reaction. Thus in this regions where the two species have sufficient residence time to compete, CO_2 get more chance to react with MDEA and this causes the concentration of H_2S in liquid to decline.

Concentration profiles for individual transferring species in gas phase along the tower were found to follow expected trends as shown in Fig. 9. No unusual or unexpected behavior was ever observed indicating thereby that our theoretical and numerical approach to modeling the process is suitable. In the liquid as shown in Fig. 10, absorptions of H_2S and CO_2 are mostly in the form of HS^- and HCO_3^- and they consumes MDEA and produces $MDEAH^+$.

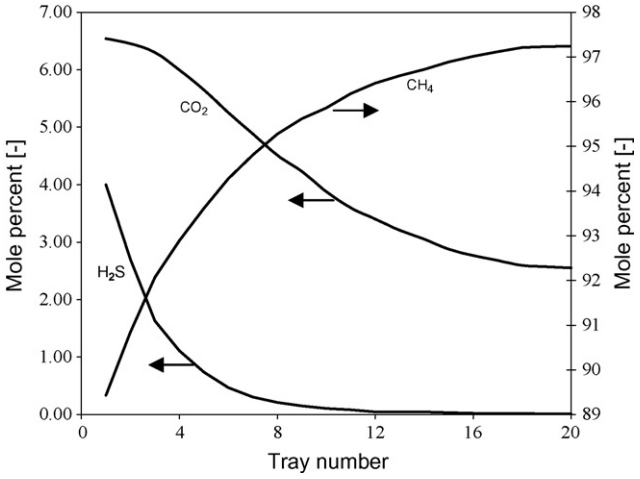

Fig. 9. Variations of average percent of transferring components in gas phase.

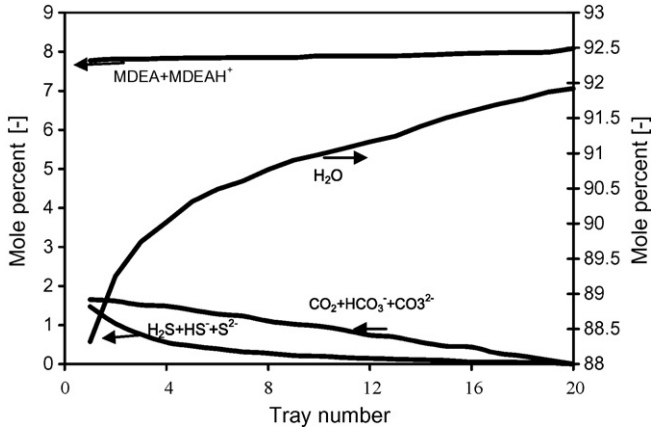

Fig. 10. Variations of average percent of transferring components in liquid phase.

Therefore concentration of MDEA + $MDEAH^+$ is constant, because it is fairly assumed that this component cannot transfer to the gas. However variations of mole fraction of MDEA + $MDEAH^+$ is due to variation of mole fraction of the other transferring components. Also, condensation of H_2O from gas to liquid and production of H_2O from reaction will increase fraction of water in liquid.

As can be seen from Fig. 10, with increasing stage number, the acid gases concentration decrease. Reaction between CO_2, H_2S and amine occurs in the liquid along the column during which the acid gases transfer to liquid. Absorption mechanism of CO_2 and H_2S is different. The constant of reaction rate between CO_2 and amine is small and consequently CO_2 absorption is low. The high concentration of the acid gases and scarcity of the amines in the bottom of the column makes two reactions of CO_2 and H_2S with amines very competitive. Because of the instantaneous reaction between H_2S and the amines, absorption of hydrogen sulfide is high and it consumes major part of the amines and leaving small fraction to react with CO_2. The absorption of H_2S is limited by the equilibrium, which is governed by the inlet liquid stream H_2S loading and temperature in addition to the molality of the alkanolamine and the system pressure. Therefore, any degree of purification of H_2S in the absence of other acid gases can easily be reached by adjusting these variables.

According to Fig. 11 temperature generally increases toward the bottom of the column. In upper trays, heat of reaction between acid

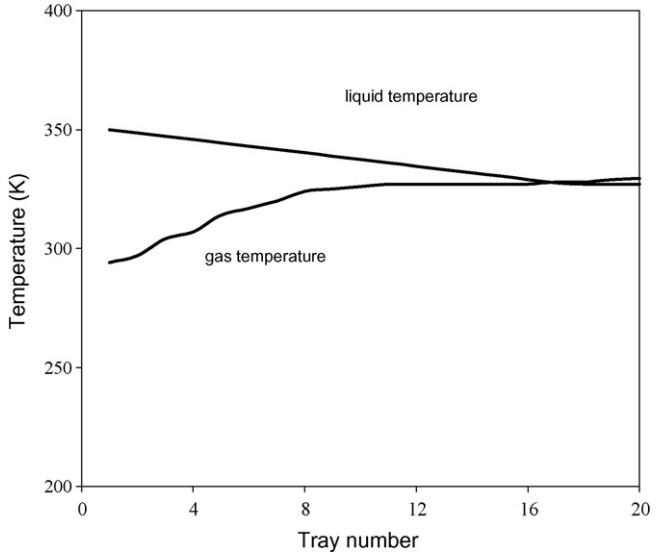

Fig. 11. Temperature profile for liquid and gas phases along the absorption tower.

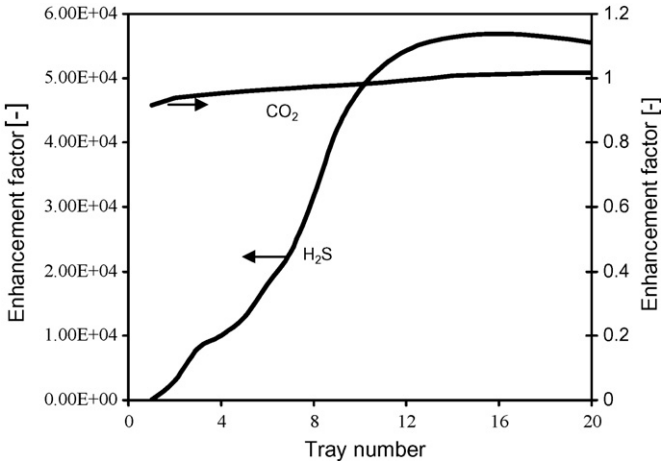

Fig. 12. Variation of averaged H_2S, CO_2 enhancement factor profile vs. stage number in absorption tower.

gases and amine has minor effect on gas and liquid temperature, because gas is approximately is free of acid gases to react with amine. Variation of liquid and gas temperature in upper trays is mainly because of heat exchange between gas and liquid flows and after fifth tray their temperature equalized. Since the major parts of reactions take place in liquid of the bottom trays, temperature of these trays increases due to heat transfer limitations.

Fig. 12 shows that the CO_2 enhancement factors are close to unity for the MDEA system. In most trays CO_2 enhancement factor is lower than unity because it cannot compete with H_2S in liquid film. However, according to the definition of enhancement factor of CO_2, it cannot be less than unity in the absence of H_2S. This indicates that CO_2 reaction with the MDEA occurs in the liquid bulk. Therefore, the process of CO_2 absorption with MDEA is controlled only by the physical diffusion of CO_2 in the liquid film. The H_2S enhancement factor is about unity at bottom of the absorber. The extreme variation of the H_2S enhancement factors along the absorber results from the competitions of H_2S and CO_2 to react with MDEA. These interactions is quantified by the numerical solution of the governing differential and algebraic Eqs. (29)–(34). The extraordinary trends cannot obviously be obtained from simple analytical enhancement factor expressions.

7. Conclusion

The presented two-dimensional model considers distributions of temperature, concentration and velocity over sieve trays in the process of absorption of acid gases, H_2S and CO_2 into solution of MDEA. This model is based on the two-film theory and considers the acceleration of mass transport due to a complex system of chemical reactions in each cell over the tray space and it is not using simplified enhancement factor concepts for a single tray. The suggested model validated with operational data of an industrial plant and it can be regarded as good mathematical model in a wide range of operating conditions. The model presented in this work indicates appreciable changes of velocity, temperature and concentration all over the trays which is originated from different mechanism of reaction of MDEA with H_2S and CO_2. This phenomenon affects temperature distribution over the tray and across the tower and also reduces enhancement factor of CO_2 below the unity which is unexpected. The magnitude of distributions of temperature, concentration and velocity increases from top to bottom of the column because flow rate of liquid increases and this intensifies the turbulence in bottom trays. The suggested model is a unique study and for the first time uses CFD frame to find the velocity, temperature and concentration distribution at different parts of a sieve tray column.

Acknowledgment

The financial support of this work by Iranian Oil and Gas Company via grant number 81-83016 is appreciated.

References

[1] N.A. Al-Baghli, S.A. Pruess, V.F. Yesavage, M.S. Selim, A rate-based model for the design of gas absorbers for the removal of CO_2 and H_2S using aqueous solutions of MEA and DEA, Fluid Phase Equilib. 185 (2001) 31–43.
[2] M. Bolhàr-Nordenkampf, A. Friedl, U. Koss, T. Tork, Modeling selective H_2S absorption and desorption in an aqueous MDEA-solution using a rate-based non-equilibrium approach, Chem. Eng. Process. 43 (2004) 701–715.
[3] S.G. Dyakonov, V.I. Elizarov, A.G. Laptev, Mass and heat transfer simulation in industrial apparatus on the base of laboratory scale model searching, Theor. Found. Chem. Eng. 27 (1993) 38–47.
[4] E.V. Murphree, Rectifying column calculations with particular reference to n-component mixtures, Ind. Eng. Chem. 17 (1925) 747–750.
[5] H. Yoshida, Liquid flow over distillation column plates, Chem. Eng. Commun. 51 (1987) 261–275.
[6] M.Q. Zhang, K.T. Yu, Simulation of two dimensional liquid phase flow on a distillation tray, J. Chem. Eng. 2 (1994) 63–71.
[7] X.G. Yuan, K.T. Yu, X.Y. You, Velocity field simulation of gas–liquid two-phase flow on sieve tray, J. Chem. Ind. Eng. (China) 46 (1995) 511–515.
[8] B. Mehta, K.T. Chuang, K. Nandakumar, Model for liquid phase flow on sieve trays, Chem. Eng. Res. Des. Trans. IChemE 76 (1998) 843–848.
[9] C.J. Liu, X.G. Yuan, K.T. Yu, X.J. Zhu, A fluid-dynamic model for flow pattern on a distillation tray, Chem. Eng. Sci. 55 (2000) 2287–2294.
[10] C.H. Fischer, J.L. Quarini, Three-dimensional heterogeneous modeling of distillation tray hydraulics, in: AIChE Annual Meeting, Miami Beach, USA, November 15–20, 1998.
[11] J.M. van Baten, R. Krishna, Modeling sieve tray hydraulics using computational fluid dynamics, Chem. Eng. J. 77 (2000) 143–151.
[12] K.T. Yu, X.G. Yuan, X.Y. You, C.J. Liu, Computational fluid-dynamics and experimental verification of two-phase two-dimensional flow on a sieve column tray, Chem. Eng. Res. Des. 77 (1999) 554–560.
[13] D.L. Bennett, R. Agrawal, P.J. Cook, New pressure drop correlation for sieve tray distillation columns, AIChE J. 29 (1983) 434–442.
[14] F.J. Zuiderweg, Sieve trays. A view on the state of the art, Chem. Eng. Sci. 37 (1982) 1441–1464.
[15] VISION 2020, 1998 separations roadmap, center for waste reduction technologies, in: AIChE Conference, New York, 1998.
[16] R. Taylor, H.A. Kooijman, J.S. Hung, A second generation nonequilibrium model for computer simulation of multicomponent separation processes, Comput. Chem. Eng. 18 (1994) 205–217.
[17] V.A. Danilov, A.G. Laptev, S.V. Karpeev, Modeling of multicomponent reactive distillation in a tray column, Acad. Open Internet J. 5 (2001).
[18] A.P. Higler, R. Taylor, R. Krishna, Modeling of a reactive separation process using a non-equilibrium stage model, Comput. Chem. Eng. 22 (1998) S111–S118.
[19] A.P. Higler, R. Taylor, R. Krishna, The influence of mass transfer and liquid mixing on the performance of reactive distillation tray column, Chem. Eng. Sci. 54 (1999) 2873–2881.
[20] A.P. Higler, R. Taylor, R. Krishna, Nonequilibrium modeling of reactive distillation: multiple steady states in MTBE synthesis, Chem. Eng. Sci. 54 (1999) 1389–1395.
[21] A. Higler, R. Krishna, R. Taylor, A non-equilibrium cell model for packed distillation columns. The influence of maldistribution, Ind. Eng. Chem. Res. 38 (1999) 3988–3999.
[22] A. Higler, R. Krishna, R. Taylor, A nonequilibrium cell model for multicomponent (reactive) separation processes, AIChE J. 45 (1999) 2357–2370.
[23] M. Ishii, Thermo-Fluid Dynamic Theory of Two-Phase Flow, Eyrolles, Paris, 1975.
[24] B.M. Mehta, Model for liquid phase flow on sieve trays, M.S. thesis, University of Alberta, Edmonton, 1997.
[25] R. Krishna, M.I. Urseanu, J.M. van Baten, J. Ellenberger, Rise velocity of a swarm of large gas bubbles in liquids, Chem. Eng. Sci. 54 (1999) 171–183.
[26] P.A.M. Hofhuis, F.J. Zuiderweg, Sieve plates: dispersion density and flow regimes, IChemE Symp. Ser. 56 (1979) 2.2/1–2.2/26.
[27] N.A. Al-Baghli, A rate-based model for the design of CO_2 and H_2S absorbers using aqueous solutions of MEA, DEA, and MDEA, PhD Thesis, Colorado school of mines, Golden, Colorado, 2001.